AGU PUBLICATIONS

JGR

Journal of Geophysical Research: Atmospheres

RESEARCH ARTICLE
10.1002/2013JD020988

Key Points:
- Complexity signatures found in the arctic tropopause and air temperature
- Tropopause and temperature variabilities exhibit different complex signatures
- Very specific time-series results supplement earlier more general studies

Correspondence to:
C. M. Hall,
chris.hall@uit.no

Citation:
Hall, C. M. (2014), Complexity signatures for short time scales in the atmosphere above Adventdalen, Svalbard, *J. Geophys. Res. Atmos.*, *119*, doi:10.1002/2013JD020988.

Received 2 OCT 2013
Accepted 2 JAN 2014
Accepted article online 4 JAN 2014

Complexity signatures for short time scales in the atmosphere above Adventdalen, Svalbard

C. M. Hall[1]

[1]Tromsø Geophysical Observatory, University of Tromsø, Tromsø, Norway

Abstract Atmospheric parameters from the troposphere above Adventdalen, Svalbard, 78°N, 16°E, are examined for signatures of complexity in their respective stochastic components over time scales from ~1 h to 1 year. Several approaches are used, all of which can estimate values of the generalized Hurst exponent, α, which can in turn be compared with each other and with similar independent characterizations, usually via the classic Hurst exponent, H, obtained from location-specific and globally averaged time series. For tropopause altitude, the stochastic component exhibits the signature of a persistent fractional Gaussian noise (fGn) with $\alpha \approx 0.75$. For surface air temperature, the indications are for fractional Brownian motion (fBm) with $\alpha \approx 1.4$. Using recent high time-resolution data from a single high-latitude location, this identification of fBm is relevant for short-term memory as opposed to findings from many other studies addressing possible long-term memory, which demonstrate fGn with $\alpha = H \approx 0.7$. Furthermore, the lack of similarity between the results for surface air temperature and tropopause altitude suggests that different underlying processes are responsible for stochastic variability.

1. Introduction

Examination of time series with the goal of identifying and quantifying scaling properties is not new to physics. *Kolmogorov* [1941] described, mathematically, the theoretical scaling relationship between sizes of structures —eddies—in well-developed turbulence as advanced by *Richardson* [1920]. In the turbulence spectrum, large structures dissipate energy by generating smaller and smaller structures and eventually heat. Distinct regimes can be identified corresponding to underlying buoyancy, inertia, and viscous forcing each characterized by power law dependence on scale size. The power-law dependencies can be predicted by dimensional analysis, and thus hypotheses as to underlying mechanisms, and then validated by observation. More recently, however, a paradigm for analysis of long-term time series has emerged in which the signal's noise, or stochastic component, is examined for self affinity. Thereafter it may or may not be possible, often by comparing scaling signatures with those of known processes, to deduce driving mechanisms a posteriori. Searching for characteristics such as long-term persistence/memory in climate (specifically, temperature) records was pioneered by, e.g., *Koscielny-Bunde et al*. [1998] and further developed by, e.g., *Eichner et al*. [2003] and *Lennartz and Bunde* [2009]. The approach is, however, notorious: *Scafetta and West* [2003], for example, proposed a linking of terrestrial temperature anomalies to solar flare intermittency via a Lévy process, sparking a heated discussion in the literature. Similarly, *Rypdal and Rypdal* [2011] find identical multifractal noise signatures in both the auroral electrojet index and the z component of the interplanetary magnetic field suggesting the existence of a physical mechanism linking intermittency in the two parameters. The aforementioned studies almost exclusively employ very long data sets, typically of 1 month time resolution with an aim to facilitating better trend analyses and prediction of future climate. Here, however, shorter (~years) data sets with higher time resolution (~hours) are analyzed using the same techniques but to search for geographically local complexity differences and similarities.

In this study, three independent approaches to time series analysis will be employed, each yielding a metric characterizing the stochastic component. As we shall see, the resulting three metrics are related and are, in turn, related to the somewhat "out-of-fashion" fractal dimension or perhaps more precisely the Hausdorff-Besicovich dimension [e.g., *Mandelbrot*, 1983]. A more contemporary approach, however, is to examine the Hurst exponent, H (originally, *Hurst*, [1951]). The first step is to isolate the stochastic component from the original time series. For the measurements that will be considered in this investigation, this involves "deseasonalizing" the data; since we have a priori knowledge of the deterministic components this deseasonalization is considered appropriate, and furthermore, the combined subsequent analyses have the possibility to reveal any

inadequacies. In this study, the data are smoothed using a boxcar of width 1 month; then this smoothed time series is subtracted from the original. The result effectively removes all variation with periods greater than 1 month, and thus seasonal, interannual, etc. periods, and, furthermore, any underlying trend. Various approaches to deseasonalization were explored by *Hall et al*. [2011a] including Butterworth filtering and subtraction of monthly climatology.

Spectral analysis (SA) is a time series analysis method that is familiar to most physicists. Normally the goal is to identify dominant periods in the data, but here since we are interested in the characteristics of the noise rather than the deterministic component, the power law dependence is obtained by linear fitting to a log-log plot of power spectral density, *S* versus frequency, *f*. Depending on the underlying data, different dependencies may emerge for different time scale ranges (analogous with the various size-scale subranges in the Kolmogorov spectrum for turbulence). We shall denote the scaling exponent (the negative of the spectral slope in log-log space) by β:

$$S(f) \propto |f|^{-\beta} \tag{1}$$

A flat spectrum indicating white noise is thus characterized by $\beta = 0$. The case of $\beta = 1$ is often referred to as "pink noise". The case where $\beta = 2$, "red noise" corresponds to Brownian motion and is alternatively called Brownian or just Brown noise. In the eventualities where power density increases with frequency, the terms blue and violet are used. For more on colours of noise, the reader is referred to *Vasseur and Yodzis* [2004]. A description of the SA method together with further references is given by *Heneghan and McDarby* [2000]; note, however, that these authors use "α" as the scaling exponent derived from the spectrum, rather than β.

The second method employed is the often-used detrended fluctuation analysis (DFA) approach [*Peng et al*., 1993]. Again, this is described in detail by, for example, *Heneghan and McDarby* [2000] together with original references. DFA is perhaps the preferred method for searching for long-term memory in data; to achieve this reliably it is necessary to establish power-law scaling (viz., as described above), investigating the constancy of spectral local slopes in a sufficient range and rejecting any exponential decay of the autocorrelation function [*Maraun et al*., 2004; *Varotsos et al*., 2013]. Then, in order to obtain a clearer view of whether long-range correlations prevail in a complex time series, DFA can be combined with a new, derived, time domain, termed "natural time" as described fully by *Varotsos et al*. [2009a] and *Sarlis et al*. [2010]. The DFA procedure itself is as follows. The stochastic component of the original time series is first used to produce a corresponding cumulative summation series (each new point is the sum of the preceding points in the original). Thereafter the cumulative summation is divided into blocks of equal size (*n*). Each of these subseries of length *n* points is then detrended either by subtracting the straight line between end-points (bridge detrending) or linear or polynomial fits (thus referred to as DFA1, DFA2, etc). Variances are calculated for each block followed by the mean *F* of these. The process is repeated for a range of block sizes (usually all possible block sizes) resulting in the function *F*(*n*). After plotting *F*(*n*) versus *n* in log-log space (as was done in the spectral analysis case) it may be possible to identify regimes exhibiting a scaling exponent α:

$$F(n) \propto n^{\alpha} \tag{2}$$

The use of α has become the norm for DFA analyses, e.g., *Delignieres et al*. [2006], as opposed to *Heneghan and McDarby* [2000] who use β. Here a simple linear detrending will be used and DFA will be used to refer to DFA(1).

The third method to be employed in this study is the lesser-used signal summation conversion (SSC) method [*Eke et al*., 2000]. The method is very similar to DFA, but the standard deviation, SD(*n*) is determined for each block/subseries (normally after linear detrending) possibly exhibiting

$$\mathrm{SD}(n) \propto n^{H_{\mathrm{SSC}}} \tag{3}$$

Where H_{SSC} is the Hurst exponent as determined by SSC.

All three methods are fully described by *Delignieres et al*. [2006]. *Hartmann et al*. [2013] also provide particularly explicit explanations for implementing the DFA and SSC methods together with a useful table of nomenclature. One fundamental difference between SA and DFA and SSC is that in the last two methods the data are cumulatively summed. If white noise is cumulatively summed, the result is a Brownian motion: the likelihoods of the motion to continue in the same direction (increasing or decreasing amplitude) or to reverse are equal. Alternatively, one can say that the successive movements or increments are uncorrelated. *Mandelbrot and van Ness* [1968] introduced the concept of fractional Brownian motions (fBm) in which successive increments are

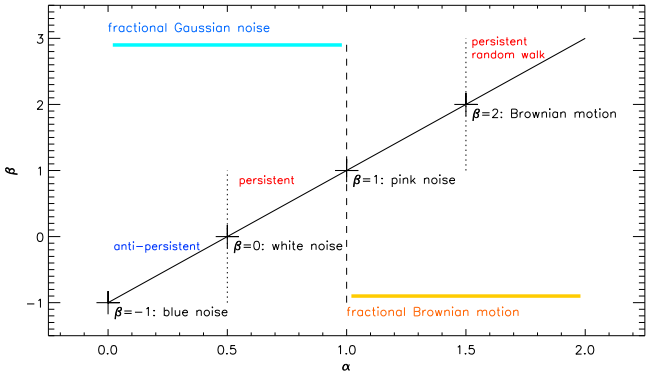

Figure 1. Relationships between slopes of the analysis methods used here: α, the generalized Hurst exponent and also the scaling exponent from the DFA, H_{SSC} from the SSC method and equivalent to α, and β from the spectral analysis.

indeed correlated. Another genre of processes is known as fractional Gaussian noise (fGn): cumulatively summing a fGn, which is stationary and time invariant in expectation value and variance, results in a corresponding fBm which is nonstationary and with temporally varying variance. Positive correlation between successive increments indicates that preceding motion is likely to continue in the next increment and negative correlation indicating that preceding motion is likely to be followed by a reversal. These likelihoods are commonly referred to as persistent and antipersistent, respectively. Any of the scaling exponents from equations (1), (2) and (3), α, β, and H_{SSC} can potentially reveal whether the noise is fGn or fBn. H, as distinct from $H_{SSC,}$ on the other hand lies in the range {0,1} wherein $H < 0.5$ is indicative of antipersistence, $H > 0.5$ is indicative of persistence and $H = 0.5$ is the special case of Brownian motion. The relationships between the three scaling exponents and H will not be derived explicitly here, and the reader is referred to *Hartmann et al.* [2013], *Heneghan and McDarby* [2000] (recalling that α and β must be interchanged), *Delignieres et al.* [2006, and references therein]. An overview is

$$\begin{gathered}\beta = 2\alpha - 1 \\ \text{For a fGn signal}: H = \alpha = (\beta + 1)/2 = H_{SSC} \\ \text{For a fBm signal}: H = \alpha - 1 = (\beta - 1)/2 = H_{SSC} - 1\end{gathered} \tag{4}$$

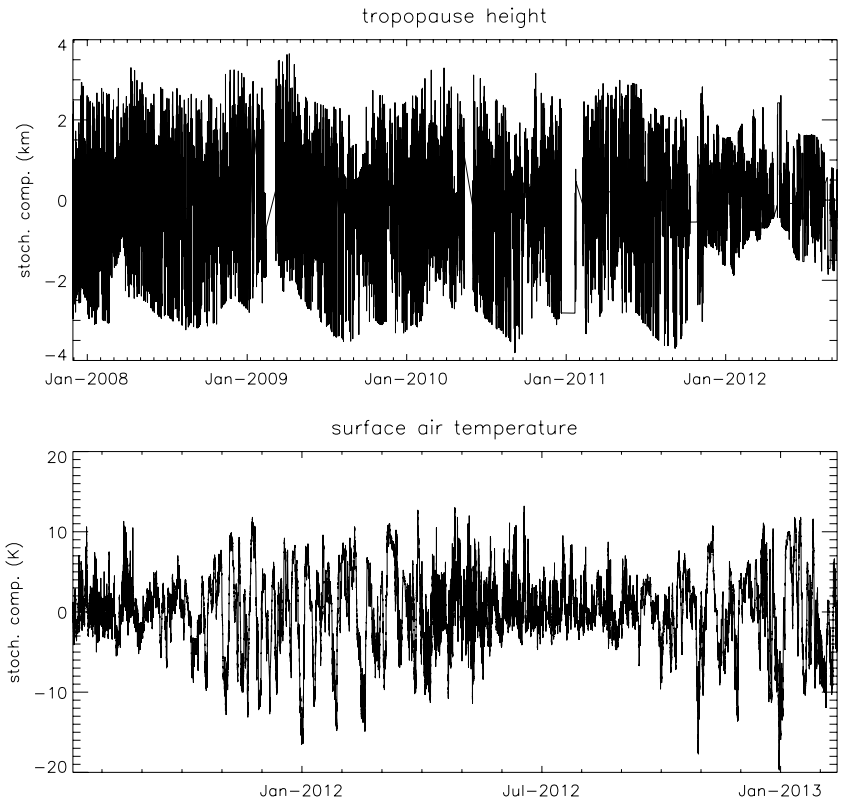

Figure 2. Stochastic components (i.e., time series after deseasonalization) of (top) tropopause heights (radar tropopause) November 2007 to December 2012 inclusive, as determined by SOUSY, and (bottom) surface air temperature August 2011 to February 2013 immediately below.

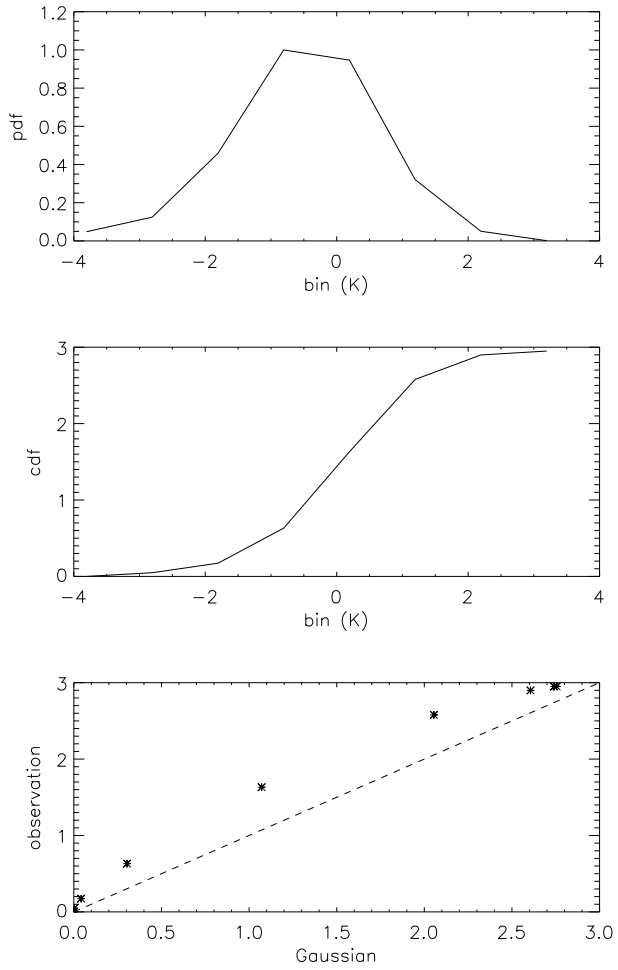

Figure 3. Statistics of stochastic component of tropopause height. (top) Probability density function (histogram); (middle) cumulative distribution; and (bottom) Q-Q plot (quantiles of distribution of observation versus those of a Gaussian distribution having the same mean and standard deviation).

These relationships are summarized pictorially in Figure 1. Also, it is worth mentioning that, applicable to fBm only, the fractal or Hausdorff-Besicovich dimension, $D = 2 - H$. One can see, therefore, that deriving D [*Grassberger and Procaccia*, 1983], although potentially yielding H does not unambiguously provide the same information as α, β, or H_{SSC}. Furthermore, α has recently been used to represent a "generalized Hurst exponent and direct classification into antipersistent fGn, persistent fGn, and fBm is performed directly from α. This is the chosen approach for the analyses that will be presented here.

2. Underlying Data

The SOUSY Svalbard radar is located in Adventdalen at 78°N, 16°E and operates automatically 24/7. A particular parameter determined by the radar is the altitude of the local radar tropopause (hereafter Z_T). The system itself, the definition of the radar tropopause and the algorithm used to determine it from the radar soundings are all described in detail by *Röttger and Hall* [2007] and *Hall et al.* [2009, 2011b]. The radar tropopause [*Gage and Green*, 1979] is closely related to the meteorological and cold-point tropopauses [*World Meteorological Organization*, 1996] as demonstrated by *Hall et al.* [2009] such that we can anticipate that any complexity signature in the radar data to be representative for the tropopause in general. One could be forgiven for assuming that in the case of a troposphere characterized by a constant lapse rate, the tropospheric thickness is directly related to the surface temperature. However, this proves not to be the case, and the temperature minimum denoting the top of the troposphere is positioned by the competing processes of tropospheric temperature and stratospheric ozone [*Highwood et al.*, 2000; *Hu et al.*, 2011]. Thus any long-term change in tropopause altitude is of particular interest for climate research because it is affected both by tropospheric warming [e.g., *Solomon et al.*, 2007; *Bèque et al.*, 2010; *Feng et al.*, 2012] and middle atmosphere cooling [e.g., *Roble and Dickinson*, 1989; *Rishbeth and Clilverd*, 1999]. These longer-term changes are addressed by, for example, *Santer et al.* [2003]. Furthermore, these effects are particularly complicated at high latitude where ozone concentration is strongly modulated by formation and breakdown of the polar vortex [*Brasseur and Solomon*, 2005; *Salby*, 1996] and by high-energy particle precipitation [e.g., *Highwood et al.*, 2000; *Zängel and Hoinka*, 2001]. As described by *Hall et al.* [2009], then, tropopause altitude is determined at a nominal 30 min resolution and the period 2008–2012 inclusive will be examined here. For a variety of reasons, including poor signal-to-noise ratio, interruption in radar operation due to power outages and occasional system breakdowns, however, the time series must be considered irregularly sampled, and this will be taken into consideration in the next section.

Originally, in order to monitor temperature indoors and outdoors at the normally unmanned radar site, surface air temperature has also been recorded since the period 2011. Again, due to occasional breakdowns and power outages, this nominally 10 s resolution time series must also be considered as irregularly sampled. Both these surface air temperature (SAT) and tropopause altitude time series were also fully described

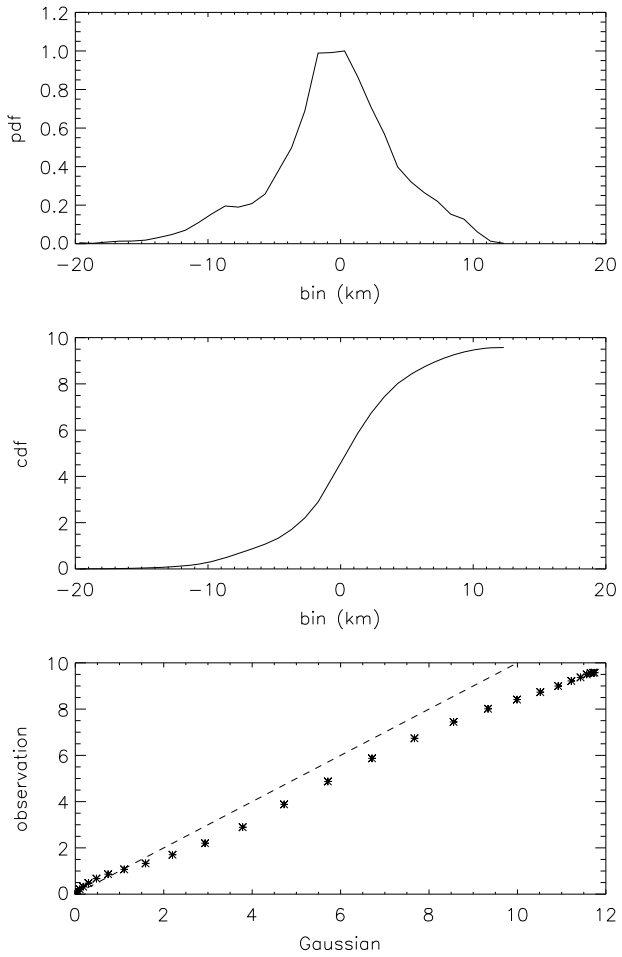

Figure 4. Statistics of stochastic component of surface air temperature. (top) probability density function (histogram); (middle) cumulative distribution; and (bottom) Q-Q plot (quantiles of distribution of observation versus those of a Gaussian distribution having the same mean and standard deviation).

recently by *Hall* [2013] and subsequently examined for similarities over short time scales. Following subtraction of time series smoothed by 1 month wide running means —the deseasonalization described in section 1, the residuals deemed to represent stochastic components (and therefore with zero mean and no overall trend) are shown in Figure 2. Short straight line segments indicate missing data: there is no interpolation here. As was mentioned by *Hall* [2013], the range resolution of 150 m in the tropopause determinations results in a degree of discretization. Furthermore, a degree of annual variability apparently remains (indicating the deseasonalization was not totally successful) and transmitter problems in November 2011 necessitated a higher altitude lower cutoff for the tropopause detection algorithm. For the SAT data, there is also a seasonal variation, but this is not in the value itself but rather in the nature of the variability, with unstable and varying temperatures during the winter and more stable conditions in summer.

Based on a priori assumptions as to driving mechanisms behind the observables, e.g., solar forcing at seasonal and solar cycle scales, corresponding time series of noise—stochastic components—have now been obtained. So do we have reason to believe that there are complexity signatures in the data? By performing quantile-quantile (Q-Q) analyses [*Wilk and Gnanadesikan*, 1968] it is possible to check for non-Gaussian distributions: quantiles of the distribution of the noise in the measured parameter are plotted against those derived from a semiempirical Gaussian distribution exhibiting the same mean and standard deviation. The investigations for tropopause height and SAT are shown in Figures 3 and 4, respectively. The probability density functions (PDFs) are shown in Figures 3 (top) and 4 (top), the cumulative density functions in Figures 3 (middle) and 4 (middle), and the Q-Q plots, including a line with slope unity, in Figures 3 (bottom) and 4 (bottom). For tropopause height, the altitude resolution of the radar is essentially inadequate, requiring bin sizes larger than the resolution; with a bin size of 1 km, all bins contain data but the density functions are sparse. Even so, there is a suggestion that the distribution is slightly skewed to the left. This is borne out by the curved nature of the Q-Q plot (although this too is sparse). See *Chambers et al.* [1963] for diagnostics of Q-Q plots. The results are more convincing, however, for the SAT noise; the PDF indicates both skew and some weight in the tails of the distribution, and the slope decreasing overall to the right indicating a skewing of the PDF to the left. The left end of the pattern being slightly above the unity slope line and the right end below the line is indicative of short tails at both ends of the distribution. Qualitatively, at least, it can be asserted that the noise in both Z_T and SAT at 78°N, 16°E are potential candidates for further analysis.

3. Data Analysis

In the preceding description of the data, it was stressed that the time series under consideration should be treated as irregularly sampled; although long data gaps are relatively few, it is incorrect to assume regularly spaced data. In performing a spectral analysis, therefore, a Lomb-Scargle periodogram analysis [*Press and*

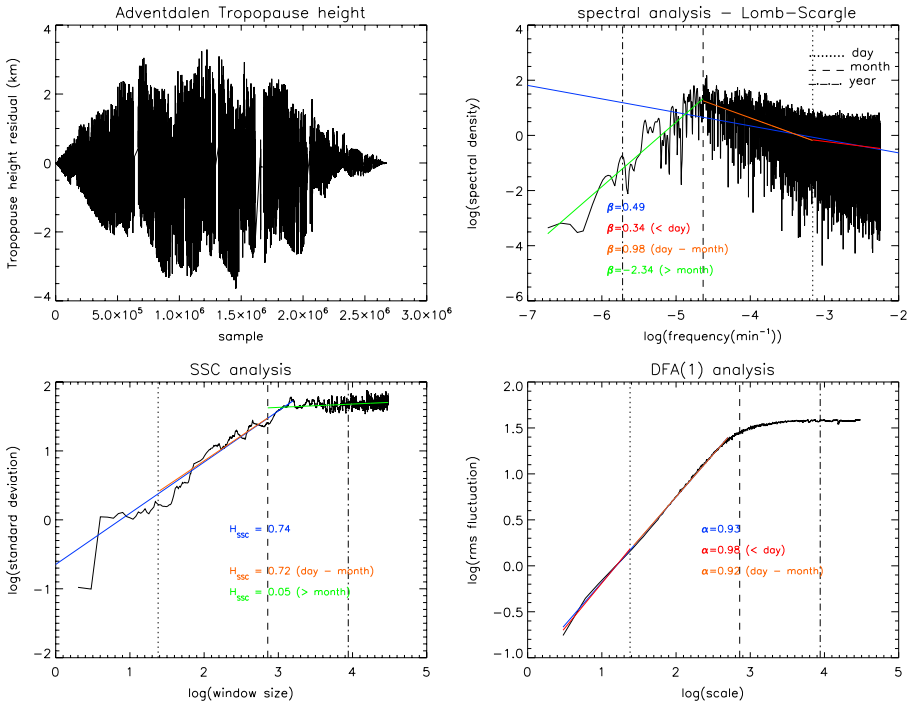

Figure 5. Tropopause height noise analyses. (top left) Time series shown in Figure 2, but now with cosine tapering and bridge detrending. (top right) Lomb-Scargle periodogram obtained from data shown in Figure 5 (top left). (bottom left) Signal summation conversion (SSC) analysis. (bottom right) Detrended fluctuation analysis (DFA). In all cases broken vertical lines indicate key time scales. Full explanations are found in the text as are explanations and interpretations of the parameters in the annotations.

Rybicki, 1989] is more appropriate than a Fourier transform. Furthermore, *Fougère* [1985] and *Eke et al.* [2000] have proposed conditioning of the time series prior to spectral analysis and frequency selection afterward. *Delignieres et al.* [2006] describe the steps in detail: conditioning by applying a parabolic window, $W(j)$, is performed, each value, j, in the series of N points being multiplied by

$$W(j) = 1 - \left(\frac{2j}{N+1} - 1\right)^2 \quad \text{for} j = 1, 2\ldots, N \tag{5}$$

Finally, bridge detrending is applied using the first and last points in the series, although strictly this should be superfluous since detrending is implicit in the deseasonalization method. The result of combining additional frequency selection with the Lomb-Scargle periodogram is somewhat unpredictable and so the entire spectrum is retained.

Six analyses follow, SA, DFA, and SSC, for each of Z_T and SAT. The signal is preconditioned using the parabolic window (equation (5)) only for SA. In each case as appropriate, the scaling exponents are obtained for all time scales, and for intraday, day-month, and greater than monthly scales. The results are shown in Figures 5 and 6. Figures 5 (top left) and 6 (top left) show the windowed signal used in the SA, Figures 5 (top right) and 6 (top right) are the SA, Figures 5 (bottom left) and 6 (bottom left) are the SSC analysis and Figures 5 (bottom right) and 6 (bottom right) are the DFA(1) analysis. In each case, vertical broken lines indicate 1 day (dotted), 1 month (dash-dotted), and 1 year (dashed) time scales, line-styles being consistent between panels. Where meaningful, fitted lines and explicit scaling exponents for each subscale and for the entire range of scales are indicated on the respective plots. For Z_T, the spectrum exhibits different scaling characteristics for scales 1 day, day-month and $>$ 1 month. The absence of significant isolated spikes can be interpreted as an indication that the deseasonalization was satisfactory. The SSC analysis gives similar results although the intraday portion is sparse and a fit has not been attempted. DFA exhibits linearity over 2 orders of magnitude for scales $<$ 1 month. For SAT the spectrum reveals isolated spikes at around 25 min and 1 day, but otherwise scaling from just under 1 month down to the 10 s sampling of the instrument. The SSC analysis exhibits convincing scaling over days to months, while for DFA scaling appears reliable only at scales shorter than 1 month, similar to the indication from the SA.

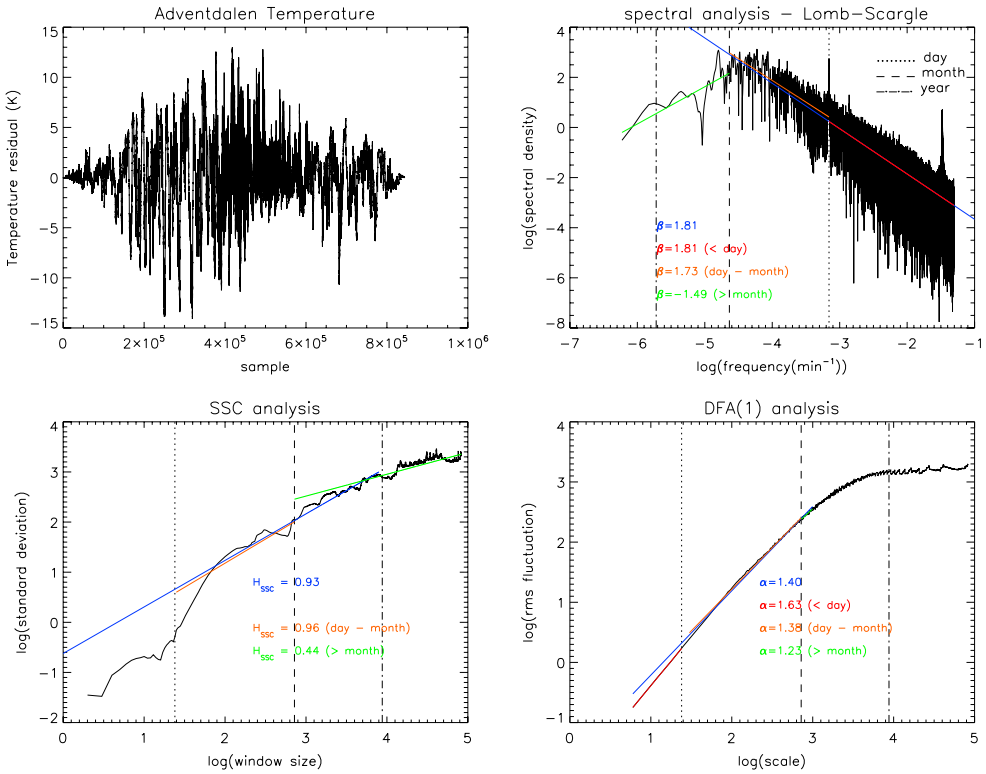

Figure 6. Surface air temperature analyses. (top left) Time series shown in Figure 2, but now with cosine tapering and bridge detrending. (top right) Lomb-Scargle periodogram obtained from data shown in Figure 6 (top left). (bottom left) Signal summation conversion (SSC) analysis. (bottom right) Detrended fluctuation analysis (DFA). In all cases broken vertical lines indicate key time scales. Full explanations are found in the text as are explanations and interpretations of the parameters in the annotations.

Even before using the relationships given in equation (4), it is evident that there is both agreement and disagreement between the three methods and the next step is to assess the reliability of the apparent scaling and to achieve this, the method described by *Theiler et al.* [1992] is used. For each of the two stochastic components (of Z_T and SAT) 100 surrogate time series are constructed using Theiler's amplitude adjusted Fourier transform algorithm (AAFT). Each surrogate exhibits the same mean, standard deviation, and Fourier transform as the observed signal but is otherwise random. The statistics obtained from the original stochastic components of Z_T and SAT are similarly obtained from each of the surrogates. For the DFA of the surrogates for Z_T, for example, the mean μ_H and standard deviation σ_H of the 100 αs are found (μ_H and σ_H are used for consistency with *Theiler et al.* [1992]). Then the significance S is defined as

$$S = \frac{|Q - \mu_H|}{\sigma_H} \tag{6}$$

where Q is the statistic from the actual data, i.e., β, α, or H_{SSC}, from Z_T or SAT. Thus, although S is dimensionless, it is essentially in units of "sigmas," and wherever it exceeds 2 we may assert that the statistic from the data is significantly different from that of the ensemble of surrogates. Since the AAFT method of generating surrogates retains the Fourier transform, we can expect S for the SA to indicate that β is not significantly different from the null hypothesis. Table 1 shows the comparisons between the scaling exponents from the surrogate ensembles for SA, DFA, and SSC. The comparison between Z_T observation and surrogate for SA is somewhat surprising since the difference is very significant; this must be attributed to the nature of the spectrum, which evidently is composed of distinct subranges each with its own scaling. Moreover, Fourier analysis is used in generation of the surrogates—an approximation due to irregularly spaced data. Without any real physical basis, dividing the surrogate spectrum into subranges would be subjective, and so the comparison will be restricted to the entire spectrum. On the other hand, the SAT SA comparison yields the expected result that the scaling exponents are nearly identical for observation and surrogates with a significance of only 0.053 sigmas. The Z_T DFA analysis of surrogates gives $\mu_H = 0.91$ as opposed to 0.93 from the observation;

Table 1. Comparison of Scaling Results for Observations and Means and Standard Deviations From Ensembles of 100 AAFT Surrogates, for Each of Z_T and SAT, and for Different Analyses

Parameter	SA (β)	DFA (α)	SSC (H_{SSC})
Z_T			
Scaling exponent from observation	0.490	0.929	0.742
Mean scaling exponent from surrogates	0.536	0.913	0.739
Standard deviation of scaling exponent from surrogates	0.0064	0.0048	0.11
Significance of scaling exponent from observation (sigmas)	7.32	3.39	0.03
SAT			
Scaling exponent from observation	1.81	1.40	0.929
Mean scaling exponent from surrogates	1.81	1.37	1.013
Standard deviation of scaling exponent from surrogates	0.054	0.0044	0.16
Significance of scaling exponent from observation (sigmas)	0.053	6.9	0.54

the difference is small, but the standard deviation σ_H is also small such that the significance is 3.4 sigmas. Similarly, for SAT the significance is 6.9 sigmas. While DFA produces a very "clean" scaling relationship, SSC does not, such that σ_H is large, resulting in H_{SSC} from the observation not being significantly different from that from the surrogate ensemble. This is the case for both Z_T and SAT, although for the latter the surrogate ensemble exhibits $\mu_H = 1.01$ such that the probability of the null hypothesis being true is ~60% [*Theiler et al.*, 1992]. To summarize, the comparisons with analyses of surrogate ensembles gives us confidence in the DFA scaling exponents, whereas SSC provides only supporting information and SA is precluded due to the method of surrogate generation.

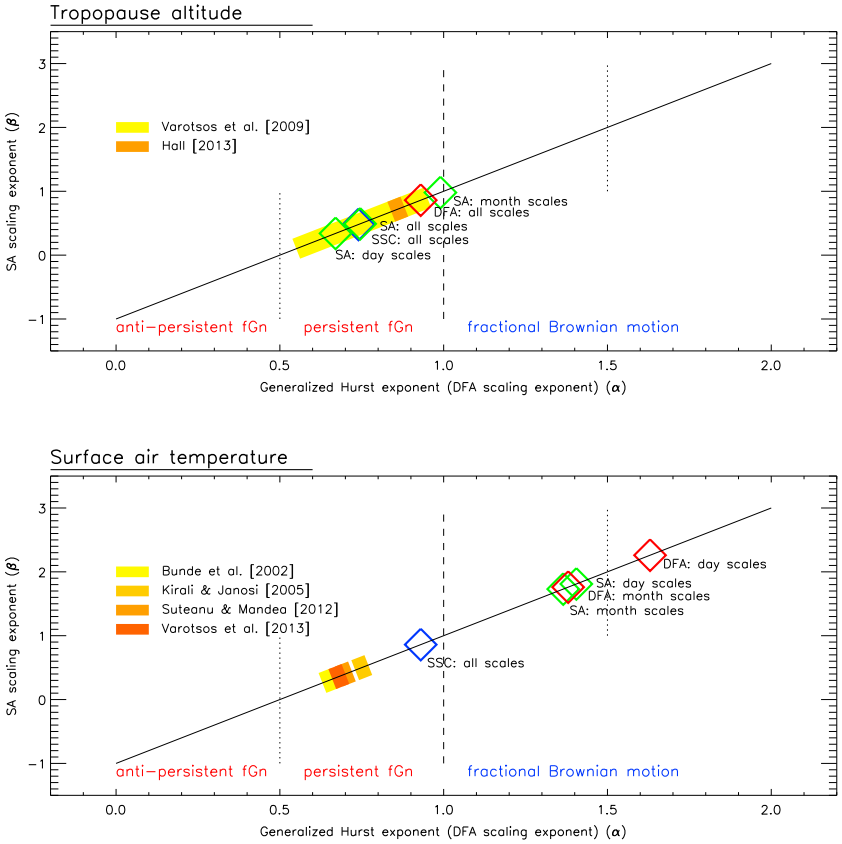

Figure 7. Analysis results displayed schematically. (top) Tropopause altitude (Z_T); (bottom) surface air temperature (SAT). The abscissa shows the generalized Hurst exponent (DFA scaling exponent) (α) and the ordinate shows the SA scaling exponent (β). α and $\beta < 1$ and > 1 indicate fractional Gaussian noise and fractional Brownian motion, respectively. Diamonds indicate results from this study (specifically from 78°N, 16°E). Colored patches show results from other studies (which may be from global data or specific locations, as discussed in the text).

4. Discussion and Conclusions

For convenience, the results from the three analyses are assembled in Figure 7. As in Figure 1.,the axes of the figure indicate the SA scaling exponent, β, and the generalized Hurst exponent or DFA scaling exponent, α, according to the relations in equation (4). For clarity, the Z_T and SAT results are shown in separate plots. Each plot can be classified thus: values of $\alpha > 0.5$ indicate persistent processes and values of $\alpha < 0.5$ indicate antipersistent processes; values of α or $\beta < 1$ indicate fractional Gaussian noise (fGn) and values of α or $\beta > 1$ indicate fractional Brownian motion (fBm). For the special case of $\alpha = 1.5$ the process is one of Brownian motion. The results from the previous section are shown on their respective panels by annotated diamonds: red, green, and blue for DFA, SA, and SSC, respectively.

For Z_T all analyses support the hypothesis that the process is fGn. From DFA, $\alpha = 0.93$, which has high significance compared to the surrogate ensemble and is in reasonable agreement with the SA result, $\alpha = 0.98$, for day-month time scales. For intraday scales, however, SA indicates $\beta = 0.34$, which biases the result of using the entire spectrum but gives $\alpha = 0.67$. Supported by the unexpected result of comparison with the surrogate ensemble, it is evident that tropopause altitude variability should be examined separately for different time scales but is otherwise characterized by persistency. Also indicated in the Figure are results from previous investigations. *Hall* [2013] found $H = 0.86$ using SA but without parabolic windowing, assuming regularly spaced observations and therefore a Fourier spectrum. *Varotsos et al*. [2009b] investigated zonally averaged observations at a variety of latitudes, finding $H = 097$. *Varotsos et al.* [2009b], however, used monthly values as their starting point and demonstrate a suggestion of zonal dependence with higher H nearer the equator, and the global average being $H = 0.9$. Given the averaging and time scale differences, the results in this study are not too dissimilar from those of *Varotsos et al*. [2009b], both indicative of persistent fractional Gaussian noise. There is no indication whatsoever of a fractional Brownian motion in the Z_T signal.

For SAT, as would be expected, there is no significant difference between SA and surrogate results. Only the all-scale SSC analysis suggests the process is fGn and with $\alpha = 0.93$; however, analysis of the surrogates shows that the confidence that this is significant compared with the null-hypothesis is only 60%. On the other hand, all other analyses, irrespective of scale, indicate fBm, with the exception of the intraday scales portion of the DFA, which indicates persistent fBm.with $\alpha > 1.5$ (the value for Brownian motion) The SA yields $\alpha \approx 1.4$ for all scales; DFA for day-month scales yields $\alpha = 1.38$ but for intraday scales $\alpha = 1.63$. The overall result is not surprising, however, because although a number of similar analyses hitherto have found persistent fGn with H between ~0.6 and ~0.8 [*Bunde and Havlin*, 2002; *Királi and Jánosi*, 2005; *Suteanu and Mandea*, 2012; *Varotsos et al*., 2013], these analyses used long time series at coarser temporal resolution to investigate, e.g., the presence of long-term memory. Strangely, classification as fGn or fBm, persistent or antipersistent does not seem to be the norm, so the figures in the aforementioned references must be examined individually, this being the basis for positioning of the annotation in Figure 7. A notable exception is the recent investigation by *Rypdal et al*. [2013] who examine characteristics of SAT from both global and local averages and at scales of months and longer. *Rypdal et al*. [2013] report global $H \approx 0.75$, local and regional $H \approx 0.65$ and with H approaching unity for locations influenced by ocean. All analysis methods employed by *Rypdal et al*. [2013] indicate fGn.

Thus, the fundamental difference between the result for SAT presented here is that a short (3 year) time series is used with sampling interval of only tens, whereas other investigations have examined longer data sets with much coarser time resolution. As stated earlier, the rationale for this study is to look for similarities (or differences) between SAT and Z_T for a very specific location, as opposed to climate- and memory-related motivations. Furthermore, the high latitude implies variation of temperature due to boundary layer inversions, katabatic winds, and generally low absolute values during both summer and winter [e.g., *Salby*, 1996]. In summer, Svalbard could be considered a location influenced by proximity to the ocean, but extensive sea ice during winter might change this classification. As for Z_T, the irregularly sampled nature of the time series has already been mentioned; apart from data gaps due to instrumental problems and failure to identify the tropopause, there are naturally occurring gaps where the tropopause is simply not defined, such as frontal passages and tropopause folds [*Nastrom et al*., 1989; *May et al*., 1991; *Alexander et al*., 2012]. In fact, isolating these features, had sufficient events been available, would result in an intermittent time series worthy of investigation.

On day-month scales, Z_T is characterized by fGn, and with $\alpha = H \sim 0.9$, and thus almost verging on pink noise. This is a somewhat higher value than the overall findings of *Varotsos et al*. [2009]; there can be a number of

reasons for this, including highly local, high-latitude source, but with the short time series, and 30 min resolution of the data for this study, such differences are to be expected. *Kantelhardt et al*. [2006] report similar findings using different hydrological data types and explain how results from shorter-term data could be modeled by an autoregressive moving-average [*Whittle*, 1951]. Furthermore, the very definition of the tropopause is different (essentially related to temperature gradient driven small scale dynamics, as opposed to the *World Meteorological Organization* [1996] definition directly related to the temperature profile) and the stochastic component of the radar tropopause may reflect this. There is a lack of similarity with the SAT signatures—this study indicating fBm and with $1.0 < \alpha < 1.5$. This is not surprising since the tropopause altitude is determined by the stratospheric temperature profile and thus ozone [*Vogler et al*., 2006, and references therein]. The effect of the ozone depends both on solar flux and on density, the latter being modulated by both dynamics and solar radiation and particle precipitation. Furthermore, the results are supported by, for example, *Tuck and Hovde* [1999] who report persistency in stratospheric temperature with $H \sim 0.84$, but ozone concentration exhibiting $H \sim 0.54$. On the other hand, vertical wind speed, influenced by shorter time scale features such as frontal passages and tropopause folds [e.g., *Sprenger et al*., 2003] exhibits fGn with $H \sim 0.25$, and therefore antipersistent.

In conclusion, therefore, tropopause altitude noise does not exhibit the same complexity signatures as surface air temperature, explicable by a combination of forcing top-down from the stratosphere in addition to the temperature structure of the underlying troposphere. Surface air temperature over short time scales exhibits complex signatures, viz., fractional Brownian motion, in contrast to fractional Gaussian noise for more geographically averaged longer time series. Considering that fBm characterizes a process that is nonstationary and with time-varying variance, it is perhaps not surprising that observations from a single location may appear as fBm, apart from being due to the temporal characteristics of the time series itself. This can particularly be the case for a very high latitude location in which insolation is absent in winter giving rise to periods of low stable temperatures with little variance interspersed with disturbances from violent depressions ("polar low"s), and unstable situations, especially during spring and autumn when rapidly changing insolation disturbs the stability, inducing katabatic winds and breakdown of nighttime inversions. Averaging, even over several relatively local time series (but especially globally) will tend to even out variances over intraannual time scales and mask any nonstationarities. Furthermore, perusal of some of the spectral analyses shown by *Rypdal et al*. [2013] reveals that over shorter time scales the spectrum tends to steepen with the scaling exponent then exceeding unity. Recall that the longer time scales are of interest for climate dynamics, whereas shorter time scales are in focus in this study, such that the characterizations of processes underlying tropopause altitude and surface air temperature do not contradict those of other studies, but rather add additional information related to scale and location.

Acknowledgments

The author would like to express gratitude for the help of Karim Kuyeng, support from the Electronics and Instrumentation group of the Jicamarca Radio Observatory, and also the staff of the EISCAT Svalbard Radar for the occasional maintenance of SOUSY.

References

Alexander, S. P., D. J. Murphy, and A. R. Klekocuik (2012), High resolution VHF radar measurements of tropopause structure and variability at Davis, Antarctica (69°S, 78°N), *Atmos. Chem. Phys. Discuss.*, *12*, 26,173–26,205, doi:10.5194/acpd-12-26173-2012.

Bèque, N., H. Bencherif, V. Sivakumar, G. Kirgis, N. Mze, and J. Leclair de Bellevue (2010), Temperature variability and trends in the UT-LS over a subtropical site: Reunion (20.8°S 55.5°E), *Atmos. Chem. Phys.*, *10*, 8563–8574, doi:10.5195/acp-10-8563-2010.

Brasseur, G., and S. Solomon (2005), *Aeronomy of the Middle Atmosphere*, pp. 646, Springer, Dordrecht, The Netherlands.

Bunde, A., and S. Havlin (2002), Power-law persistence in the atmosphere and in the oceans, *Physica A*, *314*, 15–24.

Chambers, J. M., W. S. Cleveland, B. Kleiner, and P. A. Tukey (1963), *Graphical Methods for Data Analysis*, pp. 395 , Duxbury Press, Boston, Massachusetts.

Delignieres, D., S. Ramdani, L. Lemoine, K. Torre, M. Fortes, and G. Ninot (2006), Fractal analyses for "short" time series: A re-assessment of classical methods, *J. Math. Psychol.*, *50*, 525–544.

Eichner, J. F., E. Koscielny-Bunde, A. Bunde, S. Havlin and H.-J. Schnellnhuber (2003), Power-law persistence and trends in the atmosphere: A detailed study of long temperature records, *Phys. Rev. E*, *68*, 046133.

Eke, A. H., P. Hermán, J. B. Bassingthwaighte, G. M. Raymond, D. B. Percival, M. Cannon, I. Balla, and C. Ikrényi (2000), Physiological time series: Distinguishing fractal noises from motions, *Pflügers Arch.*, *439*, 403-415.

Feng, S., Y. Fu and Q. Xiao (2012), Trends in the global tropopause thickness revealed by radiosondes, *Geophys. Res. Lett.*, *39*, L20706, doi:10.1029/2012GL053460.

Fougère, P. F. (1985), On the accuracy of spectrum analysis of red noise processes using maximum entropy and periodograms methods: Simulation studies and application to geographical data, *J. Geog. Res.*, *90*(A5), 4355–4366.

Gage, K. S., and J. L. Green (1979), Tropopause detection by partial specular reflection with very-high-frequency radar, *Science*, *203*, 1238–1240, doi:10.1126/science.203.4386.1238.

Grassberger, P., and I. Procaccia (1983), Measuring the strangeness of strange attractors, *Physica D*, *9*(1-2), 189–208.

Hall, C. M. (2013), The radar tropopause at 78°N, 16°E: Characteristics of diurnal variation, *J. Geophys. Res. Atmos.*, *118*, 6354–6359, doi:10.1002/jgrd50247.

Hall, C. M., J. Röttger, K. Kuyeng, F. Sigernes, S. Claes and J. L. Chau, (2009), Tropopause altitude detection at 78°N, 16°E, 2008: First results of the refurbished SOUSY radar, *Radio Sci.*, *44*, RS5008, doi:10.1029/2009RS004144.

Hall, C. M., K. Rypdal and M. Rypdal, (2011a) The E-region at 69°N 19°E: Trends, significances and detectability, *J. Geophys. Res.*, *116*, A05309, doi: 10.1029/2011JA016431.
Hall, C. M., G. Hansen, F. Sigernes, and K. M. Kuyeng Ruiz (2011b), Tropopause height at 78°N 16°E: Average seasonal variation 2007-2010, *Atmos. Chem. Phys.*, *11*, 5485–5490, doi:10.5194/acp-11-5485-2011.
Hartmann, A., P. Mukli, Z. Nagy, L. Kocsis, and P. Hermán (2013), Real-time fractal signal processing in the time domain, *Physica A*, *392*, 89–102.
Heneghan, C., and G. McDarby (2000), Establishing the relation between detrended fluctuation analysis and power spectral density analysis for stochastic processes, *Phys. Rev. E*, *62*(5), 6103–6110.
Highwood, E. J., B. J. Hoskins, and P. Berrisford (2000), Properties of the arctic tropopause, *Q. J. R. Meteorol. Soc.*, *126*, 1515–1532.
Hu, Y., Y. Xia, and Q. Fu (2011), Tropospheric temperature response to stratospheric ozone recovery in the 21st century, *Atmos. Chem. Phys.*, *11*, 7687–7699, doi:10.5194/acp-11-7687-2011.
Hurst, H. E. (1951), Long-term storage of reservoirs: An experimental study, *Trans. Am. Soc. Civil Eng.*, *116*, 770–799.
Kantelhardt, J. W., E. Koscielny-Bunde, D. Rybski, P. Braun, A. Bunde and S. Havlin (2006), Long-term persistence and multifractality of precipitation and river runoff records, *J. Geophys. Res.*, *111*, D01106, doi:10.1029/2005JD005881.
Királi, A., and I. M. Jánosi (2005), Detrended fluctuation analysis of daily temperature records: Geographic dependence over Australia, *Meteorol. Atmos. Phys.*, *88*, 119–128, doi:10.1007/s00703-004-0078-7.
Kolmogorov, A. N. (1941), The local structure of turbulence in incompressible viscous fluid for very large Reynolds number, *Dokl. Akad Nauk SSSR*, *30*, 9–13.
Koscielny-Bunde, E., A. Bunde, S. Havlin, H. E. Roman, Y. Goldreich, and H.-J. Schnellnhuber (1998), Analysis of daily temperature fluctuations, *Phys. Rev. Lett.*, *81*(3), 729–732.
Lennartz, S., and A. Bunde (2009), Trend evaluation in records with long-term memory: Application to global warming, *Geophys. Res. Lett.*, *36*, L16706, doi:10.1029/2009GL039516.
Mandelbrot, B. B. (1983), *The Fractal Geometry of Nature*, pp. 486, Henry Holt and Company, Macmillan.
Mandelbrot, B. B., and J. W. van Ness (1968), Fractional Brownian motions, fractional noises and applications, *SIAM Rev.*, *10*, 422–437.
Maraun, D., H. W. Rust, and J. Timmer (2004), Tempting long-memory—On the interpretation of DFA results, *Nonlinear Processes Geophys.*, *11*, 495–503.
May, P. T., M. Yamamoto, S. Fukao, T. Sato, S. Kato, and T. Tsuda (1991), Wind and reflectivity fields around fronts observed with a VHF radar, *Radio Sci.*, *26*(5), 1245–1249.
Nastrom, G. D., J. L. Green, M. R. Peterson, and K. S. Gage (1989), Tropopause folding and the variability of the tropopause height as seen by the Flatland VHF radar, *J. Appl. Meteorol.*, *28*, 1271–1281.
Peng, C. K., J. Mictus, J. Hausdorff, S. Havlin, H. E. Stanley, and A. L. Goldberger (1993), Long-range anticorrelations and non-Gaussian behavior of the heartbeat, *Phys. Rev. Lett.*, *70*, 1343–1346.
Press, W. H., and G. B. Rybicki (1989), Fast algorithm for spectral analysis of unevenly sampled data, *Astron. J.*, *338*, 277–280.
Richardson, L. F. (1920), Some measurements of atmospheric turbulence, *Philos. Trans. R. Soc. London Ser.*, *A221*, 1–28.
Rishbeth, H., and M. Clilverd (1999), Long-term change in the upper atmosphere, *Astron. Geophys.*, *40*, 3.26–3.28.
Roble, R. G., and R. E. Dickinson (1989), How will changes in carbon-dioxide and methane modify the mean structure of the mesosphere and thermosphere?, *Geophys. Res. Lett.*, *16*(12), 1441–1444.
Röttger, J., and C. M. Hall (2007), Climatology of the radar tropopause over Svalbard 2005 and 2006, in *Proceedings MST-11 Workshop India 2006*, pp. 726–729, Macmillan India Ltd., Delhi, India.
Rypdal, M. and K. Rypdal (2011), Discerning a linkage between solar wind turbulence and ionospheric dissipation by a method of confined multifractal motions, *J. Geophys. Res.*, *116*, A02202, doi:10.1029/2010JA015907.
Rypdal, K., L. Østvand, and M. Rypdal (2013), Long-range memory in Earth's surface temperature on time scales from months to centuries, *J. Geophys. Res. Atmos.*, *118*, 7046–7062, doi:10.1002/jgrd.50399.
Salby, M. L. (1996), *Fundamentals of Atmospheric Physics*, pp. 627, Academic Press Inc., San Diego, California.
Santer, B. D., et al002E (2003), Behavior of tropopause height and atmospheric temperature in models, reanalyses, and observations: Decadal changes, *J. Geophys. Res.*, *108*(D1), 4002, doi:10.1029/2002JD002258.
Sarlis, N. V., E. S. Skordas and P. A. Varotsos (2010), Nonextensivity and natural time: The case of seismicity, *Phys. Rev. E*, *82*, 021110, doi:10.1103/PhysRevE.82.021110.
Scafetta, N., and B. J. West (2003), Solar flare intermittency and the Earth's temperature anomalies, *Phys. Rev. Lett.*, *90*(24), 248701, doi:10.1103/PhysRevLett.90.248701.
Solomon, S., D. Qin, M. Manning, Z. Chen, M. Marquis, K. B. Averyt, M. Tignor, and H. L. Miller (Eds) (2007), *Contribution of Working Group I to the Fourth Assessment Report of the Intergovernmental Panel on Climate Change*, pp. 996, Cambridge University Press, Cambridge, United Kingdom and New York, NY, USA.
Sprenger, M., M. C. Maspoli and H. Wernli (2003), Tropopause folds and cross-tropopause exchange: A global investigation based upon ECMWF analyses for the time period March 2000 to February 2001, *J. Geophys. Res.*, *108*(D12), 8518, doi:10.1029/2002JD002587.
Suteanu, C., and M. Mandea (2012), Surface air temperature in the Canadian Arctic: Scaling and pattern change, *Meteorol. Atmos. Phys.*, doi:10.1007/s00703-012-0206-8.
Theiler, J., S. Eubank, A. Longtin, B. Galdrikian, and J. D. Farmer (1992), Testing for nonlinearity in time series: The method of surrogate data, *Physica D*, *58*, 77–94.
Tuck, A. F., and S. J. Hovde (1999), Fractal behavior of ozone, wind and temperature in the lower stratosphere, *Geophys. Res. Lett.*, *26*(9), 1271–1274.
Varotsos, P. A., N. V. Sarlis and E. S. Skordas (2009a), Detrended fluctuation analysis of the magnetic and electric field variations that precede rupture, *Chaos*, *19*, 023114, doi:10.1063/1.3130931.
Varotsos, C., M. Efstathiou, and C. Tzanis (2009b), Scaling behaviour of the global tropopause, *Atmos. Chem. Phys.*, *9*, 677–683.
Varotsos, C. A., M. N. Efstathiou, and A. P. Cracknell (2013), On the scaling effect in global surface air temperature anomalies, *Atmos. Chem. Phys.*, *13*, 5243–5253.
Vasseur, D. A., and P. Yodzis (2004), The color of environmental noise, *Ecology*, *84*(4), 1146–1152.
Vogler, C., S. Brönnimann, and G. Hansen (2006), Re-evaluation of the 1950–1962 total ozone record from Longyearbyen, Svalbard, *Atmos. Chem. Phys.*, *6*, 4763–4773.
Whittle, P. (1951), *Hypothesis Testing in Time Series Analysis*, vol. 120, Hafner Publishing Co., New York.
Wilk, M. B., and R. Gnanadesikan (1968), Probability plotting methods for the analysis of data, *Biometrika (Biometrika Trust)*, *55*(1), 1–17.
World Meteorological Organization (1996), Measurements of upper air temperature, pressure, and humidity. *Guide to Meteorological Instruments and Methods of Observation*, 6th edn., WMO I.12-1–I.12-32, Geneva, Switzerland.
Zängel, G., and K. P. Hoinka (2001), The tropopause in polar regions, *J. Clim.*, *14*, 3117–3139.